The Sensitivity of Hurricane Irene to Aerosols and Ocean Coupling: Simulations with WRF Spectral Bin Microphysics

BARRY H. LYNN,* ALEXANDER P. KHAIN,* JIAN WEN BAO,+ SARA A. MICHELSON,# TIANLE YUAN,@ GUY KELMAN,& DANIEL ROSENFELD,* JACOB SHPUND,* AND NIR BENMOSHE*

* *Department of Atmospheric Sciences, Hebrew University of Jerusalem, Jerusalem, Israel*
+ *NOAA/ESRL, Boulder, Colorado*
# *Cooperative Institute for Research in Environmental Sciences, University of Colorado Boulder, Boulder, Colorado*
@ *Radiation and Climate Laboratory, Goddard Space Flight Center, Greenbelt, Maryland*
& *Weather It Is, Ltd., Efrat, Israel*

(Manuscript received 15 May 2014, in final form 30 March 2015)

ABSTRACT

Hurricane Irene (2011) moved northward along the eastern coast of the United States and was expected to cause severe wind and flood damage. However, the hurricane weakened much faster than was predicted. Moreover, the minimum pressure in Irene occurred, atypically, about 40 h later than the time of maximum wind speed. Possible reasons for Irene's weakening and the time shift between maximum wind and minimum central pressure were studied in simulations using WRF with spectral bin microphysics (WRF-SBM) with 1-km grid spacing and ocean coupling. Both ocean coupling and aerosol distribution/concentration were found to influence Irene's development. Without ocean coupling or with ocean coupling and uniform aerosol distribution, the simulated maximum wind occurred at about the same time as the minimum pressure. With ocean coupling and nonuniform spatial aerosol distributions caused by aerosols from the Saharan air layer (band) and the continental United States, the maximum wind occurred about 40 h before the simulated minimum pressure, in agreement with observations. Concentrations of aerosols of several hundred per cubic centimeter in the inner core were found to initially cause convection invigoration in the simulated eyewall. In contrast, a weakening effect dominated at the mature and the decaying stages, when aerosols from the band and land intensified convection at the simulated storm's periphery. Simulations made with 3-km instead of 1-km grid spacing suggest that cloud-scale processes interactions are required to correctly simulate the timing differences between maximum wind and minimum pressure.

1. Introduction

The threat of Hurricane Irene to the U.S. mainland made news even across the Atlantic Ocean. As reported by the *Telegraph* (2011) on 25 August 2011, "the US is bracing for devastation as a large and dangerous storm roars towards the densely populated East Coast, including New York." The newspaper alerted its readers that "Hurricane Irene is forecast to become a lethal Category 4 storm with winds of 135 mph (1 mph = 0.447 04 m s^{-1}) by as early as today, according to the US National Hurricane Center (NHC)." The NHC official track forecasts were remarkably consistent and accurate in showing a path offshore from Florida and extreme eastern North Carolina (Fig. 1), along or very near the coast of the mid-Atlantic states, and into New York (Avila and Cangialosi 2011; http://www.nhc.noaa.gov/data/tcr/AL092011_Irene.pdf). Yet the maximum wind intensity of Irene was not well forecast (Fig. 2). While Irene was forecast to be a category-3 storm through landfall in North Carolina, in reality, Irene weakened to a category 1. It is notable that the surface pressure reached its minimum about 40 h later than the time of maximum wind (Avila and Cangialosi 2011). Thus, during these 40 h, tropical cyclone (TC) deepening accompanied the decrease in maximum wind. This indicates that the deepening was accompanied by a decrease in the radial pressure gradient (i.e., the size of the eyewall grew even while the minimum pressure continued dropping).

Irene may have weakened for one of several reasons. Some researchers have suggested that an incomplete eyewall replacement cycle was responsible (e.g., Zhou

Corresponding author address: Prof. Alexander Khain, Institute of Earth Sciences, Hebrew University of Jerusalem, Givat Ram, Jerusalem 91904, Israel.
E-mail: alexander.khain@mail.huji.ac.il

DOI: 10.1175/JAS-D-14-0150.1

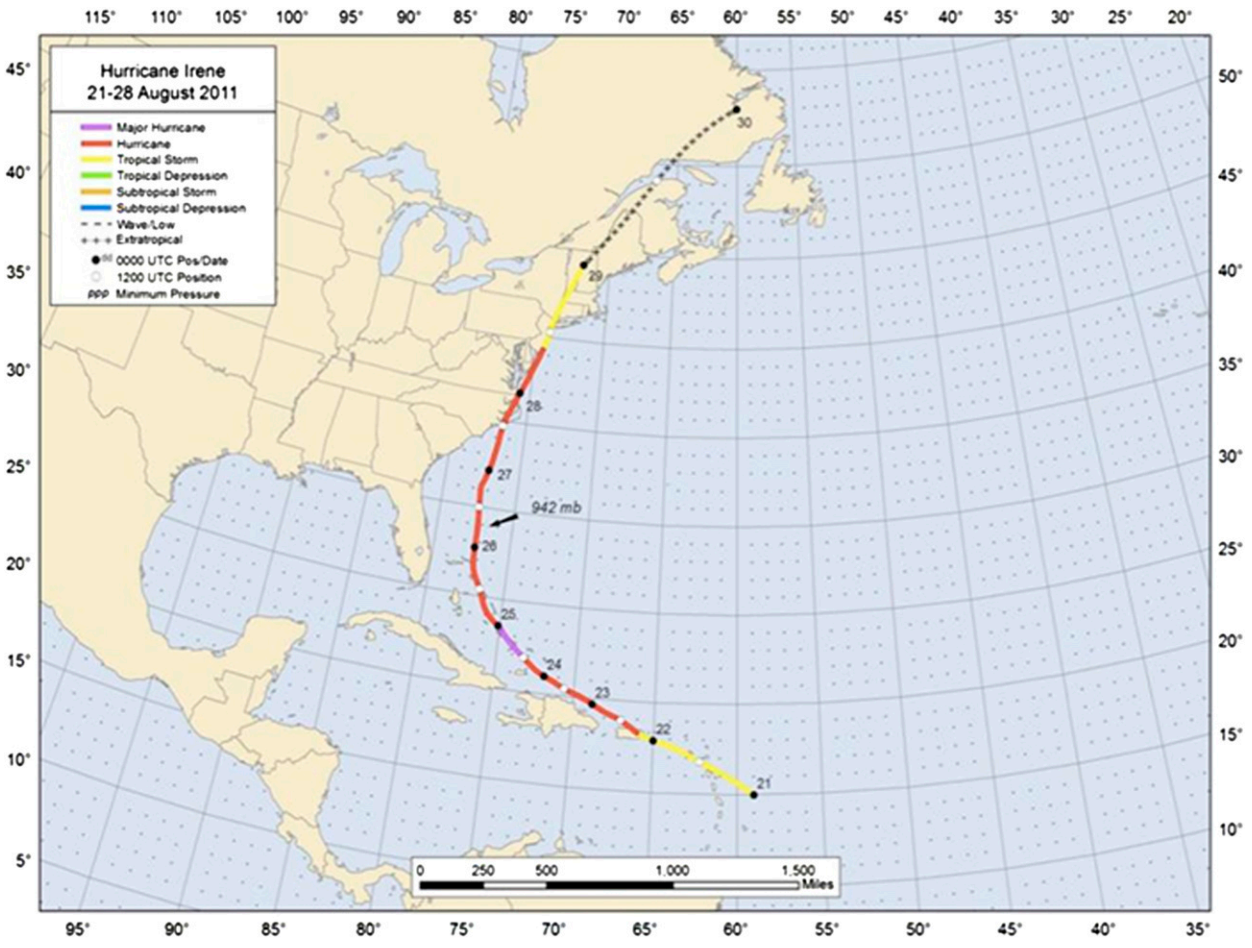

FIG. 1. The best-track positions for Hurricane Irene, 21–28 Aug 2011.

et al. 2011; Zhou and Wang 2011). From this point of view, when Irene's outer eyewall failed to undergo the contraction that typically follows inner-eyewall dissipation, restrengthening did not occur. According to observations beginning on 24 August 2011, Irene's radius grew in parallel with an intensification of its convective rainbands. An intensification of outer rainbands typically leads to TC weakening (e.g., Wang 2009). A possible reason for the observed variation of TC intensity over time is the effect of aerosols on convective clouds in the TC. We believe that it was not inconsequential that Hurricane Irene crossed a wide band of Saharan dust during its northward movement. Figure 3 (top panel) shows that Saharan-air-layer (SAL) dust impinged on Irene in three sectors at 1800 UTC 21 August 2011. Most of the dust was not observable by satellite 54 h later (0000 UTC 24 August 2011), but it is still seen to Irene's north in a cloud-free area (Fig. 3, bottom panel). This indicates that the dust seen at the earlier time was likely absorbed into Irene's circulation.

In large-scale models, the effects of aerosols on the atmosphere are typically related to their effects on the radiative budget both directly (direct effect) or indirectly via the effects on cloud microphysics (indirect effects) (Tao et al. 2012). In this study, we investigate the indirect effect of aerosols on tropical storm development or aerosol impacts on cloud microphysical process. It is now well recognized that aerosols tend to intensify tropical convection (Khain et al. 2005, 2008a, 2010; Khain 2009; Rosenfeld et al. 2008; Tao et al. 2012). Moreover, since aerosol-induced convection invigoration leads to the intensification of rainbands (and even lightning activity), it can even foster initial TC development (Jenkins et al. 2008; Jenkins and Pratt 2008; Khain et al. 2008b; Zhang et al. 2009; Hazra et al. 2013; Herbener et al. 2014).

In contrast, when a TC approaches land, a significant amount of continental aerosol is available as cloud condensational nuclei (CCN), which can lead to an intensification of convection at the TC periphery and to TC weakening (Khain et al. 2008b, 2010; Khain and

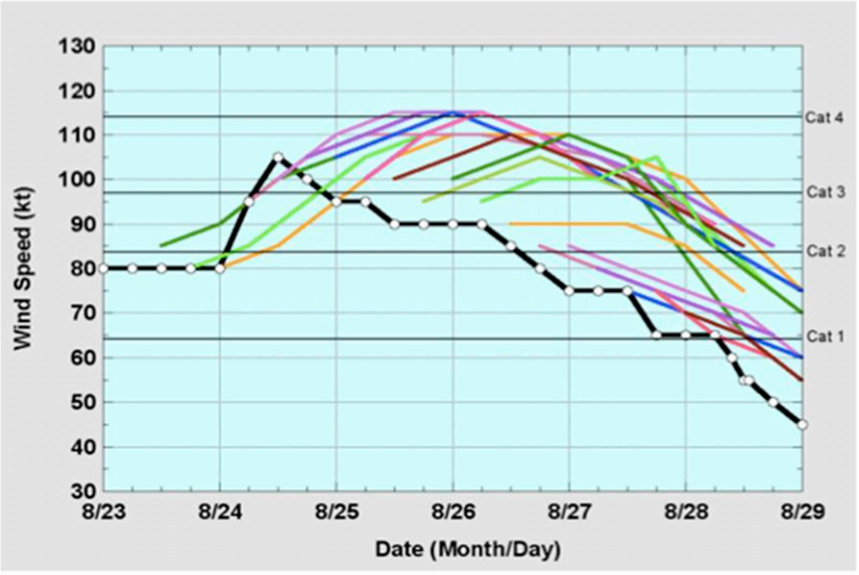

FIG. 2. Official NHC intensity forecasts for Irene every 6 h from 1200 UTC 23 Aug to 0600 UTC 28 Aug.

Lynn 2011; Rosenfeld et al. 2012; Cotton et al. 2007, 2012). According to Khain et al. (2010), aerosol-induced convection invigoration in Hurricane Katrina's periphery led to an increase by more than 10 mb (1 mb = 1 hPa) in surface pressure (and corresponding weakening of wind speed in the vicinity of the eyewall).

A decrease in sea surface temperature (SST) caused by a mixing of the oceanic upper layer and upwelling may also substantially decrease TC intensity (Khain and Sutyrin 1983; Khain 1984; Bender et al. 1993; Bender and Ginis 2000; Ma et al. 2013). The cold wake induced by a TC may not only weaken the TC but may also foster the expansion of the storm circulation. In the case of Irene, comparatively high initial values of SST were associated with a very low depth of the oceanic mixing layer of just 15 m (Fig. 4). Thus, the mixing of the surface ocean water layer during the storm's movement would be expected to lead to a dramatic decrease in SST (I. Ginis 2013, personal communication).

In this study, we evaluated the possible contribution of two physical mechanisms on the weakening of Irene: (i) aerosol effects on cloud microphysics and convection; and (ii) effects of TC–ocean interaction leading to an SST decrease. Simulations of Irene's track and intensity were carried out using the Advanced Research Weather and Forecasting Model, version 3.4 (Skamarock and Klemp 2008; for details, see http://www2.mmm.ucar.edu/wrf/users/docs/user_guide_V3/contents.html), mostly with 1-km grid spacing, using 6-h reanalysis data from the Global Forecast Systems model. Cloud dynamics and microphysics were simulated using spectral (bin) microphysics (SBM) (Khain et al. 2010). Pollard et al.'s (1972) one-dimensional ocean model [described further by Davis et al. (2008)] was used to test the potential impact of ocean coupling on Irene's intensity. The paper is structured as follows. Section 2 discusses the model setup, while section 3 presents the results of the simulations. A summary and conclusions are given in section 4.

2. The model and experimental design

The nested-grid WRF (version 3.4) includes SBM (Khain et al. 2010) as an add-on microphysical option, and this code has also been included in version 3.6. The grid spacing was 9 km × 9 km in an outer grid, where there were 700 × 700 grid elements. The first inner (moving) nest had 3 km × 3 km grid spacing and 300 × 300 grid elements. The innermost grid had 1 km × 1 km grid spacing with 499 × 499 grid elements. In each of the simulations, there were 30 vertical layers, with the finest resolution in the boundary layer.[1] The simulations began at 0000 UTC 21 August 2011 and ended at 0000 UTC 28 August 2011. The initial position of the

[1] A simulation was set up to test the sensitivity of the results to using additional vertical levels toward the top of the atmosphere. As identified by Fierro et al. (2009) and Chen et al. (2011), finer grid spacing at the top of the model domain can influence the development of the upper-level secondary circulation that "vents" the TC. In a test, the minimum surface pressure of the simulation with 47 layers was about 3–4 mb lower than in the simulation with 31 levels. The sensitivity of the TC minimum pressure and maximum wind to the vertical resolution turns out to be much weaker than the sensitivity of TC minimum pressure and maximum wind to SST changes or to the initial aerosol distribution.

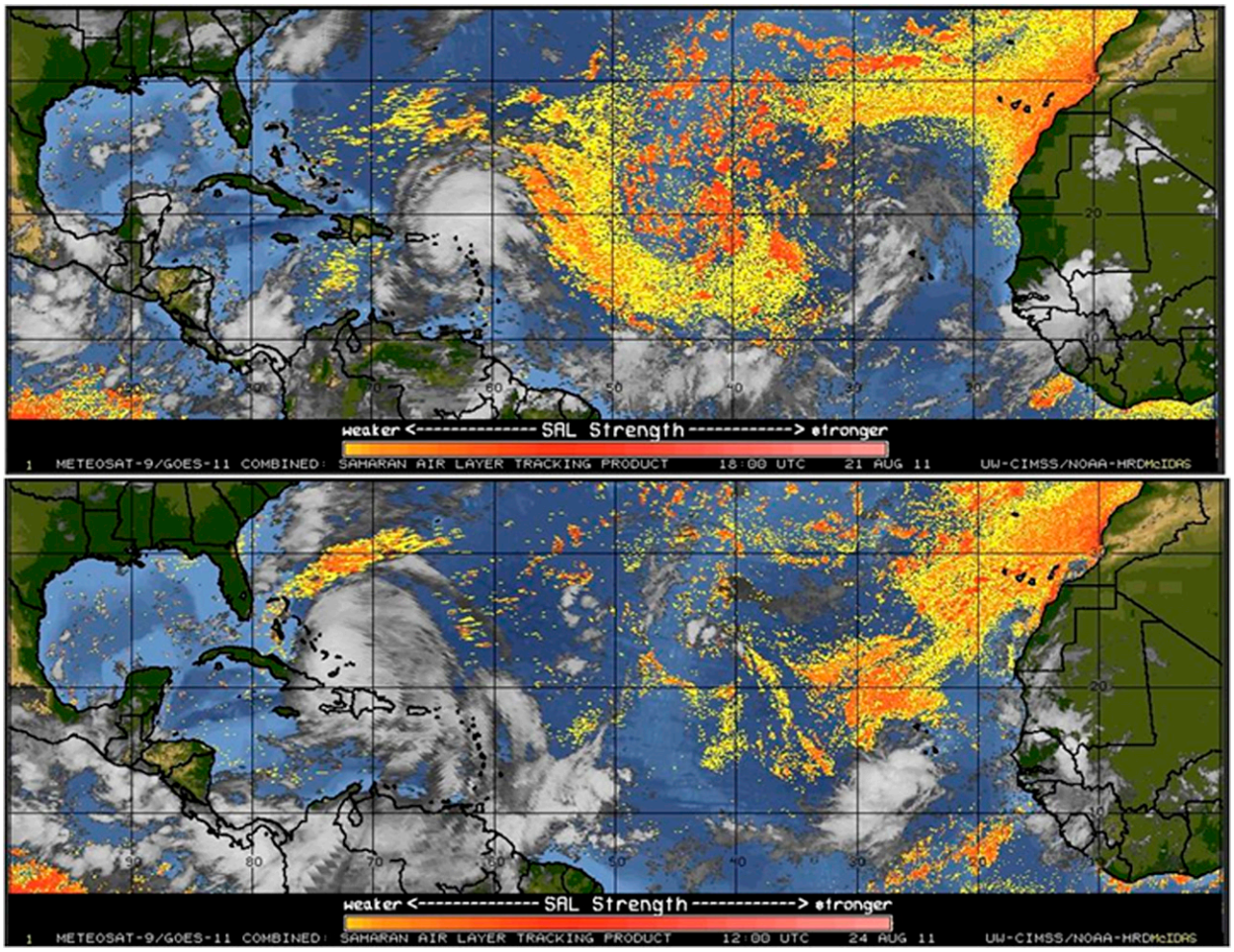

FIG. 3. Dry-air, Saharan-air-layer maps from the University of Wisconsin–CIMSS (http://tropic.ssec.wisc.edu) for (top) 1800 UTC 21 Aug and (bottom) 0000 UTC 24 Aug 2011.

storm was about 15°N and 60°W (southeast of the Lesser Antilles islands), and the final position was about 40.7°N, 74°W (just east of New York City, New York), 192 h later. Each of the simulations used the GFS analysis fields as boundary conditions, which included grid nudging of the temperature, winds, and specific humidity above the boundary layer in the outer 9-km grid (http://nomads.ncdc.noaa.gov/cgi-bin/ncdc-ui/define-collection.pl?model_sys=gfsanl&model_name=gfsanl&grid_name=4). The 2.5-order closure of the Mellor–Yamada–Nakanishi–Niino boundary layer scheme, version 2 (MYNN2), was used to calculate the surface layer and boundary layer flux processes[2] (Nakanishi 2000; Nakanishi and Niino 2009).

The SBM scheme is described by Khain et al. (2010) and based on the SBM scheme included in the Hebrew University Cloud Model in Khain et al. (2004). The SBM is based on solving a system of size distribution functions for drops, low-density ice hydrometeors (aggregates or snow), and high-density ice particles (graupel/hail) size distributions. The shapes of the particle size distributions (PSD) change with time and space as a result of advection, diffusion growth–evaporation, deposition–sublimation, collisions, sedimentation, and freezing–melting, etc. Each size distribution is defined on the logarithmically equidistant doubling mass grid and contains 33 mass bins. The mass of the minimum bin corresponds to droplets of 2-μm radius. The thirty-third bin corresponds to the mass of 4-mm-radius drops. This mass grid is suitable for tropical clouds in which drops and ice particles are comparatively small.

Diffusional growth–evaporation of drops and deposition–sublimation of ice particles is calculated by solving an equation system for the equation of diffusional

[2] We tested the impact of the choice of boundary layer scheme on the forecast minimum pressure and maximum wind using other available options. Using MYNN2 gave the most realistic forecast results, when compared to commonly used surface layer and boundary schemes referred to as the Yonsei University (YSU; first order) and MYJ (1.5 order).

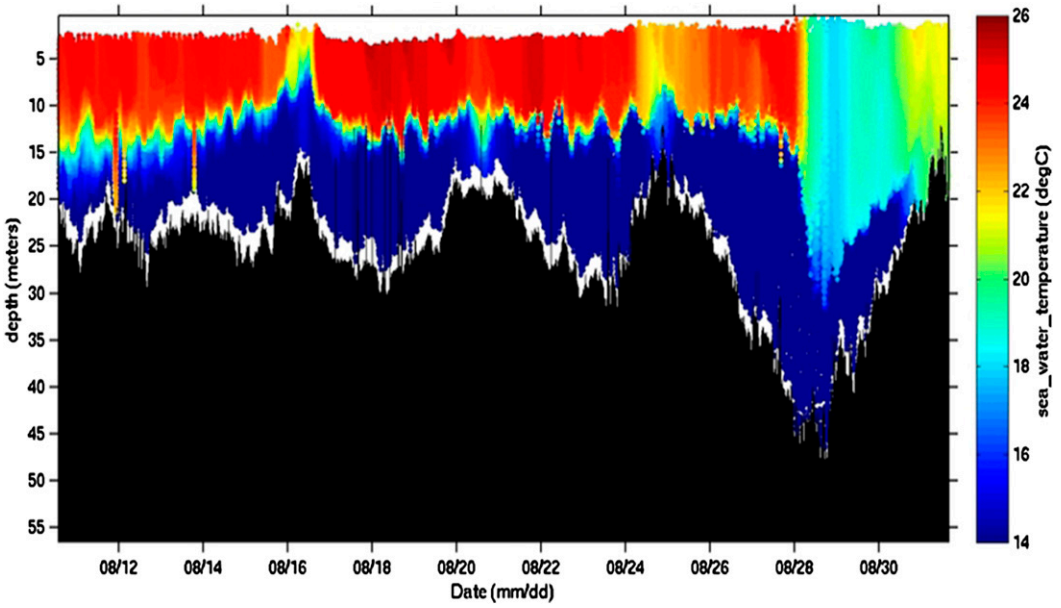

FIG. 4. Time series of seawater temperature from observation from the Mid-Atlantic Regional Association Coastal Ocean Observing System (MARACOOS) (http://maracoos.org/irene/?p=305).

growth and equations for supersaturation over water and ice. As a result, the changes in the values of supersaturation during the diffusion growth are taken into account.

The changes of PSDs by collisions between particles of all types are calculated by solving stochastic collision equations using collision kernels calculated by Pinsky et al. (2001) and Khain et al. (2001). The nucleation of pristine ice particles is described using the scheme by Meyers et al. (1992).

Freezing of drops is described using the semiempirical formula of probability freezing, according to which the freezing rate is proportional to drop mass (Bigg 1953). Bigg's (1953) formula is used for temperatures lower than −20°C. For higher temperatures, the formula by Vali (1994) is used. Regarding frozen drops, those with radius below 100 μm are converted to small aggregates (snow). Larger frozen drops are converted to hail/graupel type. The model also describes the processes of ice nucleation.

To calculate the effects of soluble aerosols (CCN), an aerosol size distribution is used. The aerosol size distribution also contains 33 bins. The maximum size of dry aerosol particles is equal to 2 μm. The aerosols are assumed to be soluble and consist of NaCl. The shape of the aerosol size distribution changes with time and space as a result of advection, diffusion growth/evaporation, and activation to drops.

The process of droplet nucleation is described using the Köhler theory, with some changes for large CCN [see Khain et al. (2000) for details]. Using supersaturation calculated at each time step, a critical CCN size is calculated so that CCNs with radii exceeding this critical radius are converted to droplets. In this case, the CCN size distribution in corresponding bins becomes equal to zero. No aerosols return to the atmosphere in case of cloud/raindrop evaporation. Since the humidity in hurricanes is high, the process of raindrop evaporation is not efficient and cannot greatly increase CCN concentration.

The initial size distribution of dry aerosol particles serving as CCN was derived from the empirical expression for CCN activation spectra written as $N_{CCN} = N_o S_w^k$, where S_w is supersaturation over water in percent, N_{CCN} is the concentration of CCN activated under supersaturation S_w, N_o is the concentration of CCN activated under supersaturation $S_w = 1\%$, and k is a slope parameter characterizing the shape of CCN size spectrum. The quantities N_o and k are measured constants.

The main goal of the numerical experiments was to find the reasons for the unexpected decrease in the maximum wind and the time shift between the maximum wind and minimum surface pressure. We consider two physical mechanisms: TC–ocean coupling and the effects of aerosols on deep convective clouds and the subsequent feedbacks on Irene's intensity. The list of experiments (Exps.) is presented in Table 1. Ocean coupling was included in Exps. 1, 3, 4, and 5 but not in Exp. 2.

To evaluate the effects of the SST decrease as a result of TC coupling, we conducted several simulations using

TABLE 1. List of experiments.

Experiment	Model resolution (km)	Aerosols	Ocean coupling
Exp. 1	1	Continental aerosols over the land, a 3-km-depth Saharan dust band, maritime aerosols over the sea and within the central area with grid spacing ≥ 3 km	Yes
Exp. 2	1	As in Exp. 1	No
Exp. 3	1	Low (maritime) aerosols everywhere	Yes
Exp. 4	1	As in Exp. 1, but low aerosol concentration over land	Yes
Exp. 5	1	As in Exp. 4, but continental aerosols were assumed in the internal TC area	Yes
Exp. 1_3 km	3	As in Exp. 1	Yes
Exp. 2_3 km	3	As in Exp. 1	No

the above-mentioned WRF one-dimensional ocean model and bulk microphysics. According to the results of preliminary simulations, the utilization of the oceanic mixed layer of 15 m gave a realistic SST cooling of about 4°–5°C (I. Ginis 2013, personal communication). Thus, in the SBM TC–ocean coupled simulations, the depth of the oceanic mixed layer was set equal to 15 m. The initial SST was obtained from the GFS reanalysis data files. In Exp. 2 and Exp. 2_3 km (without the 1D SST model), the SSTs were updated every 6 h using the data from 6-hourly GFS reanalysis files. In the other simulations with the 1D SST model, only the initial SSTs at 0000 UTC 21 August were used, and the SSTs were calculated thenceforth using the 1D model. The lapse rate below the mixed layer was 0.14 K m^{-1}.

The configuration of the initial aerosol distributions is shown in Fig. 5. The design of the aerosol distribution over the computational area in Exp. 1 is presented in Fig. 5a. In Exp. 1, high aerosol concentration was assumed over land (continental aerosols) and low aerosol concentration over the ocean. A band of Saharan-air-layer aerosols with aerosol layer depth of 3 km was assumed stretching east to west along the southern half of the domain.[3] In Exp. 1 the maritime aerosol size distribution was assumed in the central area covered by grids with resolutions of 3 and 1 km. The goal of implementing the clean zone around the TC center was to mimic the initial conditions indicated by the satellite that aerosols were not initially within Irene's inner zone.

In Exp. 2, the initial aerosol setup was as in Exp. 1, but there was, as noted, no ocean coupling. The goal of Exp. 2 was to reveal the effect of ocean coupling on the TC intensity and structure. In Exp. 3, the initial aerosol concentration was uniformly maritime with ocean coupling (Fig. 4b). The goal of this experiment was to reveal the effects of variations in aerosol spatial distribution (as represented by aerosols over land and within the Saharan air layer) on the TC intensity.

In Exp. 4, the setup was as in Exp. 1, but aerosols over land (outside the band) were assumed to be maritime (Fig. 4c). The goal of this experiment was to reveal the effects of continental aerosols on the TC intensity and structure.

In Exp. 5, the setup was as in Exp. 4, but continental aerosols were also included within the initial storm circulation area (i.e., within the 3- and 1-km simulation domains). Additionally, two simulations were done with the same setup as Exp. 1 and Exp. 2, but with 3-km grid spacing (Exp. 1_3 km and Exp. 2_3 km). The goal of these simulations was to evaluate the effects of model resolution on the intensity and microphysical structure of the simulated TC.

The maritime aerosols were specified with $N_o = 100\,\text{cm}^{-3}$ and $k = 0.4$. In dustlike continental conditions, N_o was set to $4000\,\text{cm}^{-3}$, with $k = 0.9$. The initial aerosol concentration decreased exponentially with height above 2 km in each of these simulations. An additional simulation was done with intermediate-like continental conditions, where N_o was set to $2000\,\text{cm}^{-3}$. Some simulations were done using 3-km grid spacing.

3. Results

All of the storms tracked very close to the observed track (not shown), so differences in the TC intensity between simulations were due to either differences in the aerosol configurations or ocean coupling.

a. *Effect of aerosols and TC–ocean coupling on Irene's intensity and structure*

Figure 6 shows the SST fields in observations and Exp. 1 prior to (23 August) and after the passage of Irene (28 August). The utilization of a 1D ocean model

[3] Saharan dust stretched from 10° latitude to 30° latitude (based on an examination of MODIS data). CALIOP lidar data was used to determine that a constant aerosol mixed layer extended from about the surface through a 3-km depth. Above this layer, the dust concentration was initially zero.

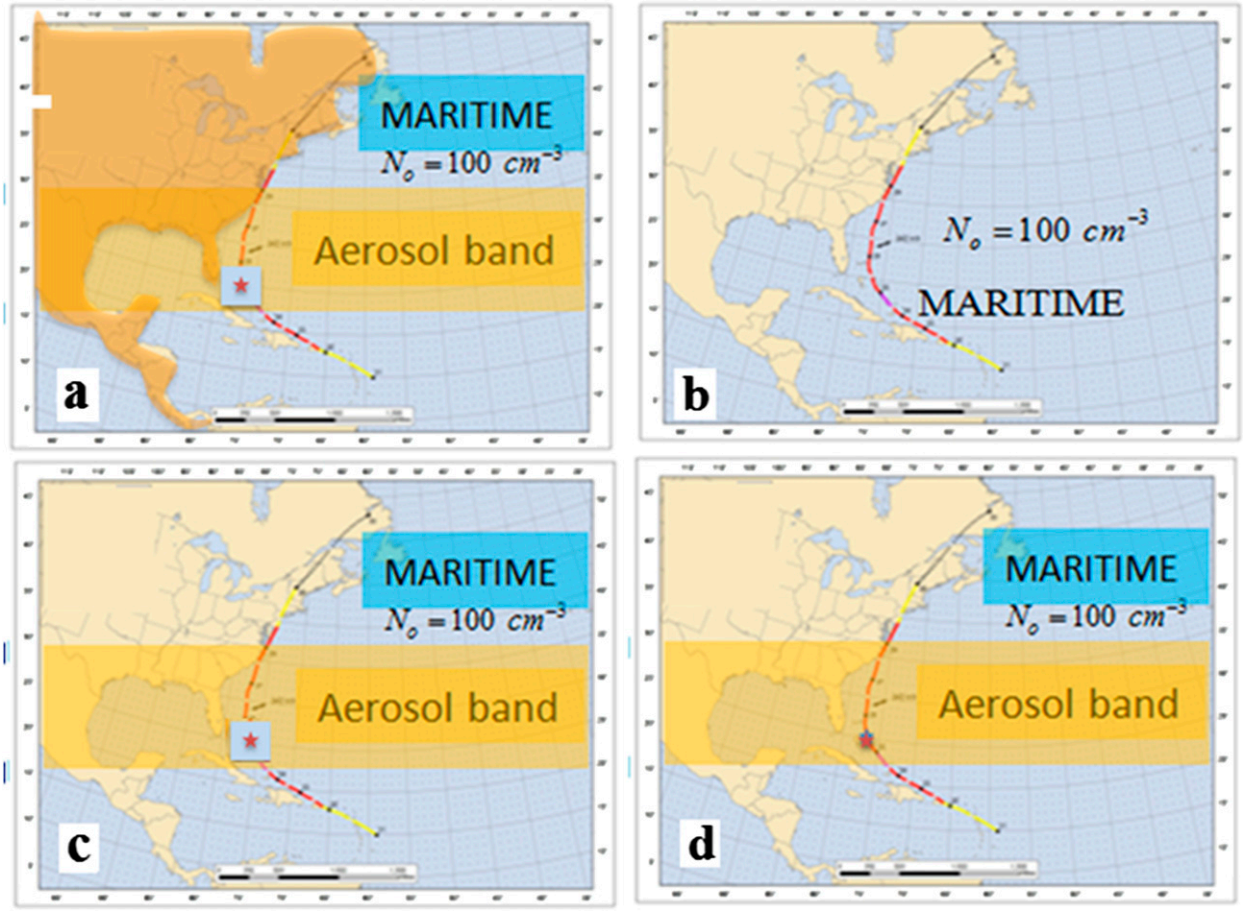

FIG. 5. Four configurations of the initial spatial distributions of aerosols in numerical simulations: Exps. (a) 1, (b) 3, (c) 4, and (d) 5. Asterisk shows initial location of Irene in the simulations. The aerosol configuration in Exp. 2 is as in (a). The small blue area in the inner TC zone in (d) indicates the zone with maritime aerosols.

allowed the reproduction of a reasonable facsimile of the observed cold band in the ocean. While the observations show a decrease in the SST to between 23°–24°C, the SSTs in the simulation decreased to between 25°–26°C. We attribute this smaller SST decrease to the fact that the 1D ocean model does not describe the physical process of convergence and its associated upwelling of cold water (as might be simulated with a 3D ocean model). The SST results shown were typical of other simulations made with ocean coupling.

Figure 7 shows the time evolution of maximum wind (Figs. 7a,b) and minimum pressure (Figs. 7c,d) for Exps. 1–5. With the exception of Exp. 2, (i.e., no ocean coupling), each of the simulated minimum pressures were within 5–10 mb of the observed minimum pressure value. Yet, of all the experiments, Exp. 1 (Fig. 7a) was the most realistic, because it simulated the correct time of the maximum wind versus the time of minimum pressure. As previously noted, it includes ocean coupling and was designed to represent (in an idealized sense) the impact of the SAL intrusion and aerosols from land on the tropical storm structure. That is, the hurricane in this simulation developed in a relatively pristine environment, but, within about 48 h, dust entering the eyewall circulation invigorated convection in the TC center. However, by the time the storm approached the U.S. mainland, aerosols entering the storm's periphery (not shown) led to relative storm invigoration in the outer rainbands, leading to its eventual weakening (as discussed further below).

In contrast, the simulated Irene in Exp. 2 without ocean coupling was much stronger than in the observations. The maximum winds in this simulation soon exceeded 100 knots (kt; 1 kt = 0.51 m s^{-1}) and remained so for more than 100 h. In fact, the largest difference between observations and simulated wind speed was ~35 kt, while the differences in minimum pressures

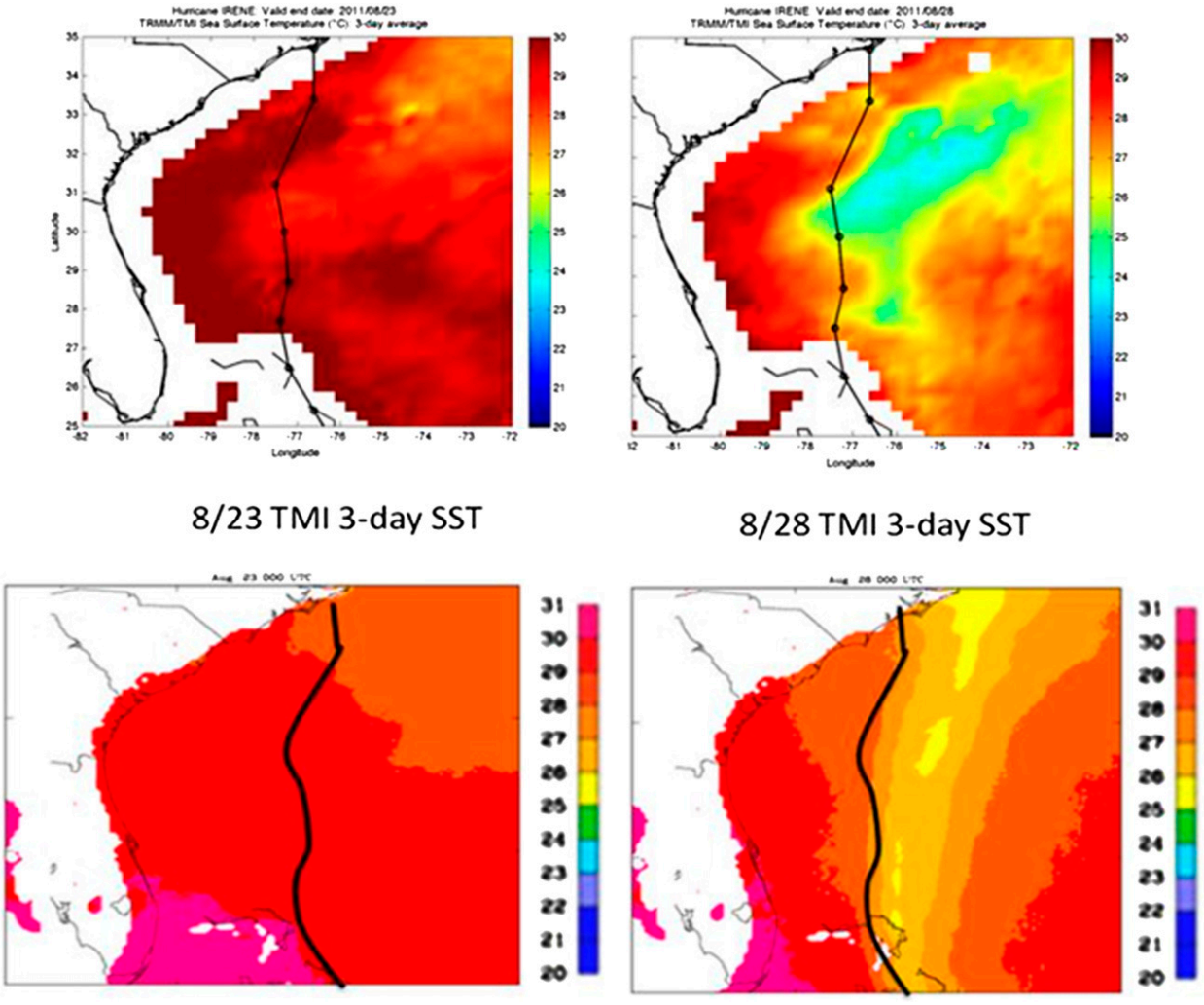

FIG. 6. The fields of SST (left) before and (right) after the passage of Irene, according to (top) observations (I. Ginis 2013, personal communication) and (bottom) forecast. Note that the observations show 3-day-averaged SST fields.

were between 25 and 35 mb. When the simulated storm developed in a maritime (uniform) environment (Exp. 3), the maximum wind exceeded 100 kt for almost 70 h. The maximum wind speed and minimum pressure were about 25 kt higher and 15 mb lower than in Exp. 1, and the maximum wind occurred at about the time of minimum pressure. Uniformly increasing the aerosol concentration did not impact the relative timing of the maximum wind–minimum pressure (not shown). Instead, we see that the spatial distribution of aerosols and ocean coupling both have substantive impacts on TC development.

Comparison of time dependencies of maximum wind and pressure minimum in Exp. 4 and Exp. 5 shows that the initial presence of aerosols in the TC central area invigorated convection and intensified the simulated Irene more quickly than without aerosols in the area of initial TC development. The invigoration of tropical convection through an increase in the CCN concentration was simulated in many studies and reported in observations (Khain 2009; Khain et al. 2010; Rosenfeld et al. 2008; Tao et al. 2012). An increase in the CCN concentration leads to the formation of a larger number of cloud droplets, which efficiently absorb water vapor. Because of low collision efficiency, small droplets produce raindrops slower and at higher levels than in the case of low CCN concentration.

As a result, the droplets in cases of high CCN concentration grow by diffusion (condensation) over a longer time and ascend to higher levels with more efficient freezing, as compared to cases of low CCN concentration. All these processes lead to a stronger latent heat release than in the case of low CCN concentration. Exp. 5 had stronger maximum winds than Exp. 4, since

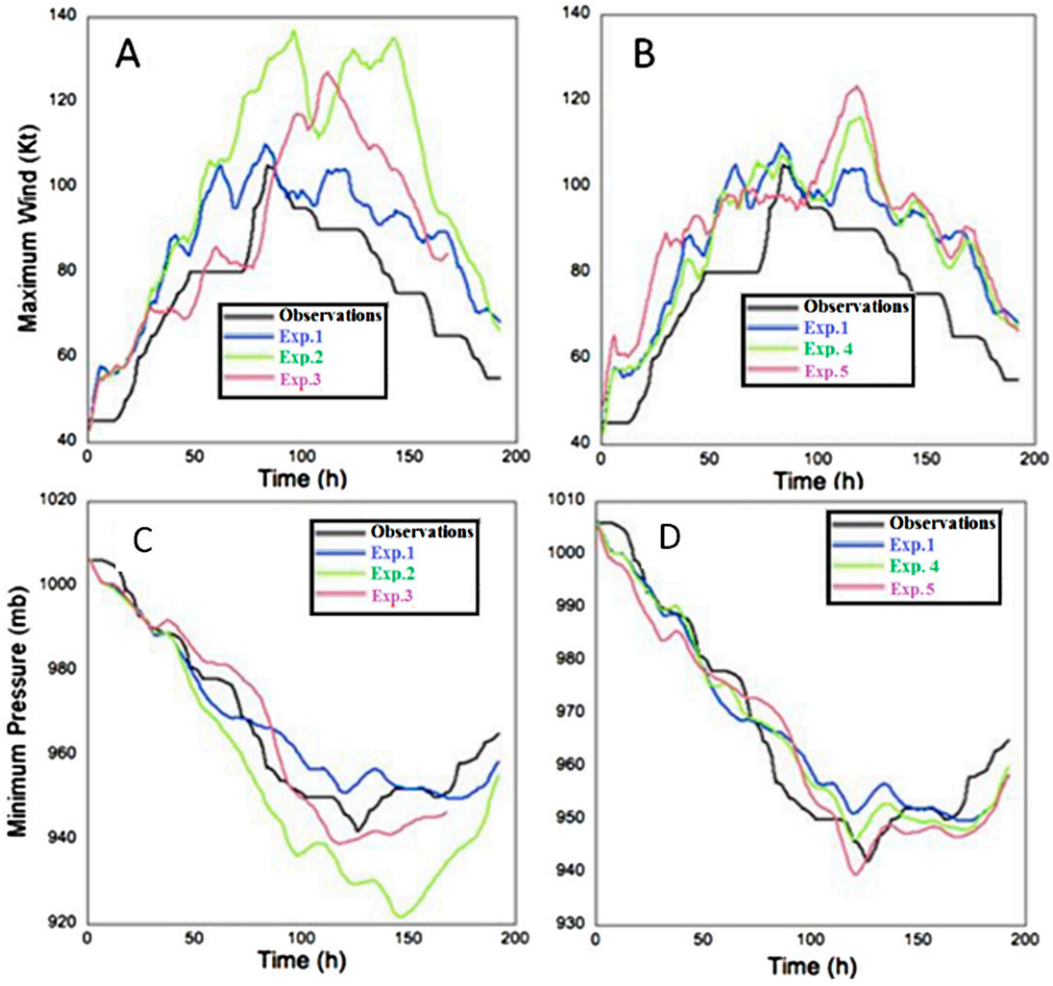

FIG. 7. Time dependencies of (a),(b) maximum wind and (c),(d) minimum pressure in different experiments described in Table 1 with (left) Exps. 1, 2, and 3 and (right) Exps. 1, 4, and 5. Observed time dependencies are also presented. Exp. 1 with and Exp. 2 without ocean coupling and initially banded (high concentrations of) aerosols. Exp. 3 with ocean coupling, but with low-concentration (initially uniform maritime) aerosols. Exp. 4 was similar to Exp. 1, but without aerosols over land, while Exp. 5 was like Exp. 4, but with high aerosol concentration initially in the center of the storm.

the former intensified more quickly at the beginning of the simulation than the latter.

Figure 8 shows the relationships between maximum wind and minimum pressure from Exps. 1, 2, and 3. A comparison of these curves shows that ocean coupling and aerosol impact (on the periphery convection) together act to produce a more realistic maximum wind–minimum pressure relationship than without ocean coupling or with ocean coupling but with uniform initial aerosol concentrations. It is interesting to note that Exp. 2 produced a double maximum in the maximum wind and minimum pressure hysteresis curve (to be discussed further in Section 4). The appearance of the maximum in the wind speed at about $t = 80$ h is seen also in Fig. 7a. However, the maxima of wind speed in Exp. 2 were too high because of no ocean coupling. The formation of the first wind maximum indicates that the presence of aerosols in the storm center zone invigorating the storm was enough to lead to subsequent intensifications. An analysis of the results in Figs. 7 and 8 indicates a very important role played by aerosols on the intensity of the TC at all stages of its evolution.

Figs. 9–13 explain the mechanisms by means of which aerosols affect Irene's structure. Figure 9 illustrates differences in the field of vertical velocity at a height of 9 km in Exps. 1 and 3 caused by differences in the aerosol concentrations and distributions. At the developing stages (0500 UTC 25 August; 105 h into the simulations), vertical velocities in the eyewall in Exp. 1 were larger, and the radius of the eyewall (as indicated by the vertical

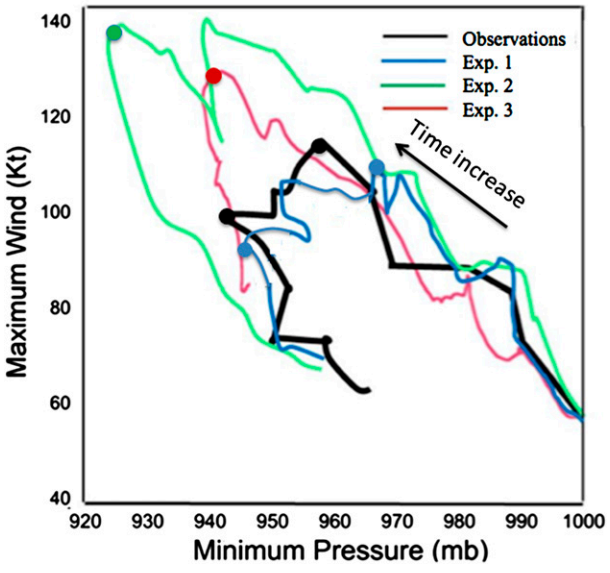

FIG. 8. The maximum wind velocity–minimum pressure relationships in Exp. 1 (with initially banded aerosols and continental aerosols). Exp. 2 was similar to Exp. 1, but without ocean coupling. Exp. 3 had ocean coupling but initially uniform maritime aerosols. Circles denote the points of minimum pressure and maximum wind. In Exp. 2 (Exp. 3) the minimum pressure and the maximum wind take place in one time instance, which is denoted by one green (red) circle of maximum wind–minimum pressure dependencies. In Exp. 1, maximum wind and minimum pressure are reached at different time instances, which are denoted by two circles. The results reached in Exp. 1 (when effects of continental aerosols are taken into account) agree well with observations.

velocity field) was smaller than in Exp. 3 (cf. Figs. 9a,b and Figs. 9c,d at 1200 UTC 25 August). Between 0000 and 0800 UTC, aerosols penetrated the inner core (eyewall) of the simulated TC in Exp. 3 from the Saharan dust band on the storm's northern side (not shown). At the mature stage (0800 UTC 26 August) the values of the maximum velocity in Fig. 9f decreased in the eyewall but increased over a large area at the northern periphery of the TC because of aerosol-induced invigoration (through greater latent heat release associated with diffusional growth of many cloud drops). The structure of vertical velocity in Exp. 1 (Fig. 9f) reflects the process of the second eyewall formation and the weakening of the innermost eyewall. Moreover, because of the aerosol intrusion in the periphery, the secondary eyewall does not contract to the size of the former eyewall (see below). In contrast, no substantial changes in the structure of the simulated TC in Exp. 3 took place (Fig. 9e).

The difference in the structure of the inner TC core in Exp. 1 and Exp. 3 is clearly seen in the field of rainwater mixing ratio [rainwater content (RWC)]. Figure 10 shows fields of RWC at the altitude of 4.5 km at different time instances. At 0500 UTC 25 August, the aerosol-penetrated eyewall in Exp. 1 led to the intensification of convection in the eyewall and to a smaller eye radius. At 1200 UTC, aerosols entering the storm in Exp. 1 intensified the rainbands outside of the eyewall and increased the number of the bands, compared to Exp. 3 (again because of greater latent heat release associated with the higher aerosol concentrations in Exp. 1 vs Exp. 3). By 0800 UTC 26 August, Exp. 1, but not Exp. 3, shows a large rainband spiraling around and far from the storm center. Moreover, the radial size of the inner rainband in Exp. 1 was much larger than in Exp. 3.

The differences in the structure of the convection in Irene's inner core are well seen in the radially averaged wind speed and sea level pressure versus radial distance for Exp. 1 and Exp. 3 (Fig. 11). At 50 and 70 h, the maximum wind speeds in Exp. 1 (Fig. 11a) were about 5 m s^{-1} higher than in Exp. 3 (Fig. 11b), while minimum pressures are about 5 mb lower in Exp. 1 (Fig. 11c) compared to Exp. 3 (Fig. 11d). The radius of the maximum wind in each experiment was between 30 and 40 km. At 100 h, the maximum wind in Exp. 3 was about 10 m s^{-1} higher than in Exp. 1, and the minimum pressure was about 10 mb lower. The radius of the maximum wind in Exp. 1 was less than 50 km, while there was a secondary maximum in Exp. 1 just beyond 50 km.

At 120 h, both experiments produce their peak maximum wind speeds, and each was located at about 50 km (Figs. 11a,b). Yet the minimum pressure in Exp. 3 was about 10 mb lower than in Exp. 1, while the maximum wind speed in Exp. 3 was about 10 m s^{-1} higher than in Exp. 1. Moreover, Exp. 1 had a secondary peak about 110 km from the storm center associated with the formation of the secondary eyewall, with wind speeds a few meters per second higher than those in Exp. 3. At 150 h, the maximum wind speed in Exp. 1 reached a maximum value about 100 km from the storm center. However, the internal maximum related to the original eyewall disappeared. During this time, aerosols entered from the continental United States on its southwestern side. In contrast, the wind speed increased smoothly in Exp. 3 until about 75 km from the storm center. No formation of the secondary eyewall was found in Exp. 3.

Figures 11c and 11d clarify the mechanism leading to time shift between maximum wind and minimum pressure. One can infer that the formation of the secondary eyewall at a larger radius in Exp. 1 led to a decrease in the radial pressure gradient. Thus, the decrease in the pressure in the TC center was accompanied by a decrease in maximum wind. In Exp. 3, one can infer that the decrease in the central pressure was accompanied by an increase in the pressure gradient. As a result, in Exp. 3,

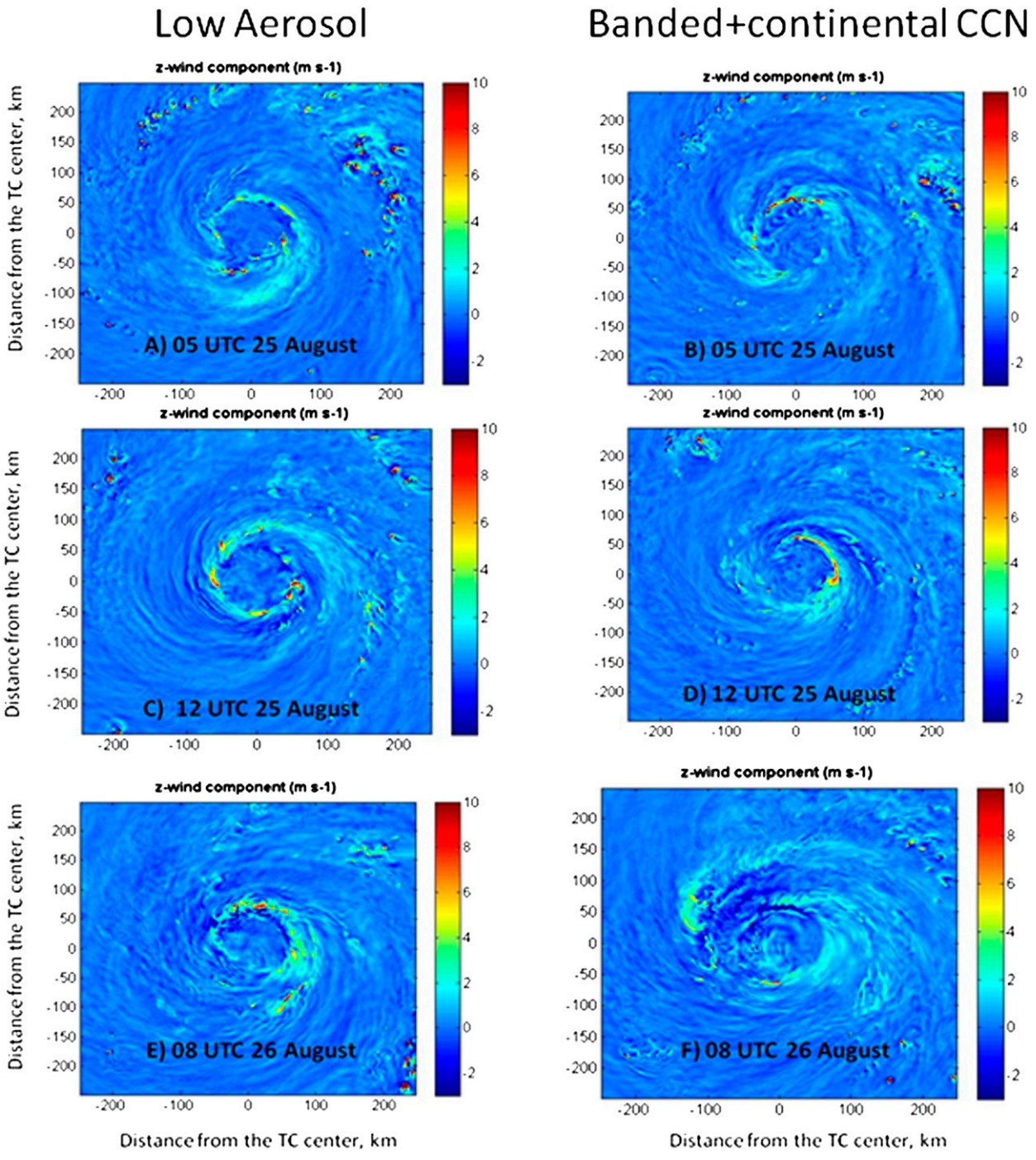

FIG. 9. Horizontal cross sections in the field of vertical velocity ($m\,s^{-1}$) at $z = 9$ km in (a),(c),(e) low-aerosol and (b),(d),(f) high-aerosol (banded) simulations at (top) 0500 UTC 25 Aug, (middle) 1200 UTC 25 Aug, and (bottom) 0800 UTC 26 Aug.

a decrease in the pressure was accompanied by an increase in the maximum wind.

The changes in the dynamical structure of the inner TC core were seen not only in the fields characterizing warm microphysics, but also in those characterizing ice microphysics. We present two examples. Figure 12 compares SSM/IS 91-GHz color composite images at 2336 UTC 25 August (Fig. 12a) and 1040 UTC 26 Aug 2011 (Fig. 12b) with the fields of simulated total mass content of ice crystal and aggregates from a model setup similar to Exp. 1 and Exp. 3 (the grid spacing was 3 km, but the results were very much like those with 1-km grid

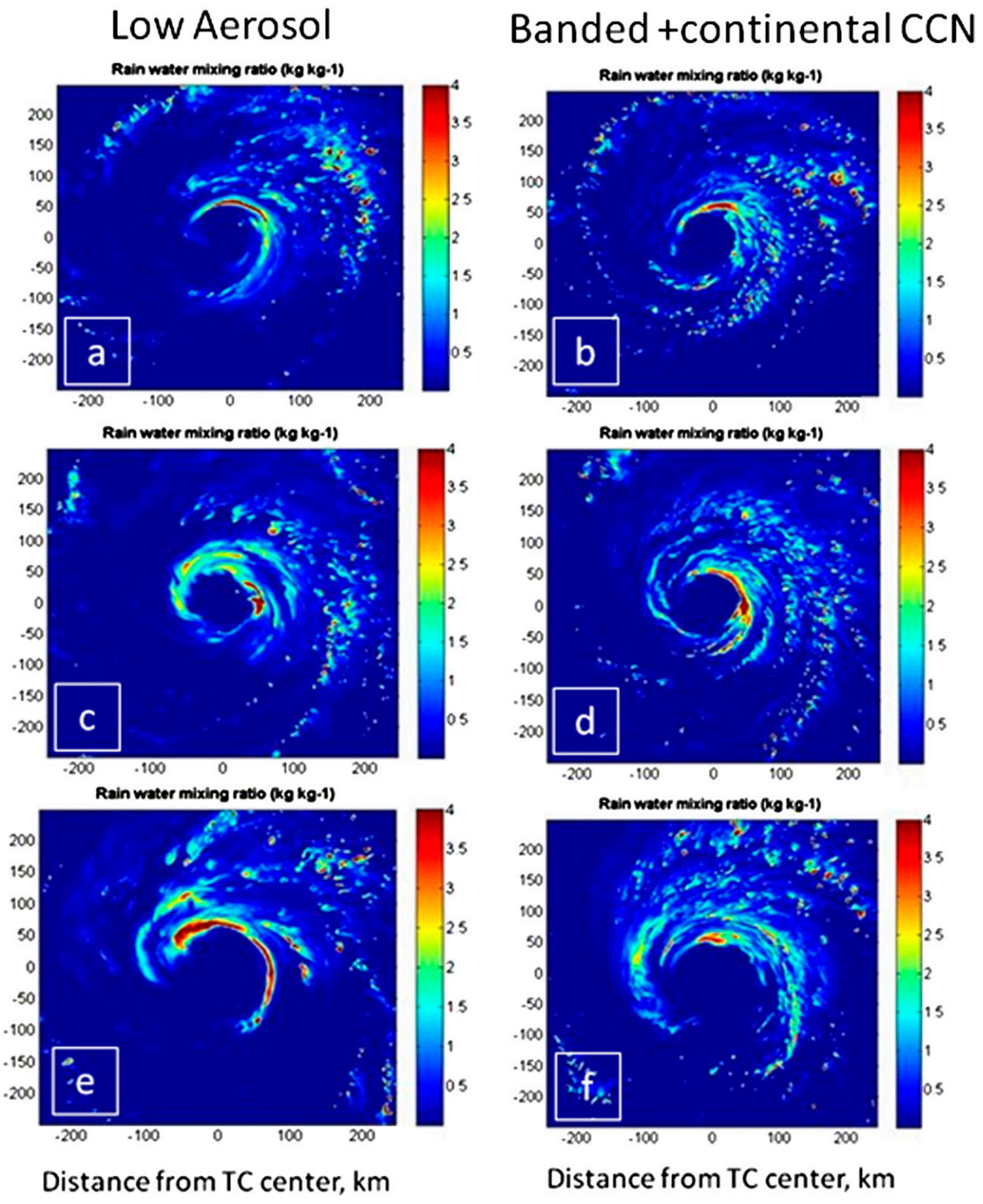

FIG. 10. Fields of rainwater mixing ratio (kg kg^{-1}) at the altitude of 4.5 km in simulations with (a),(c),(e) low CCN concentration (Exp. 3) and (b),(d),(f) high banded CCN concentration (Exp. 1) at (top) 0500 UTC 25 Aug, (middle) 1200 UTC 25 Aug, and (bottom) 0800 UTC 26 Aug.

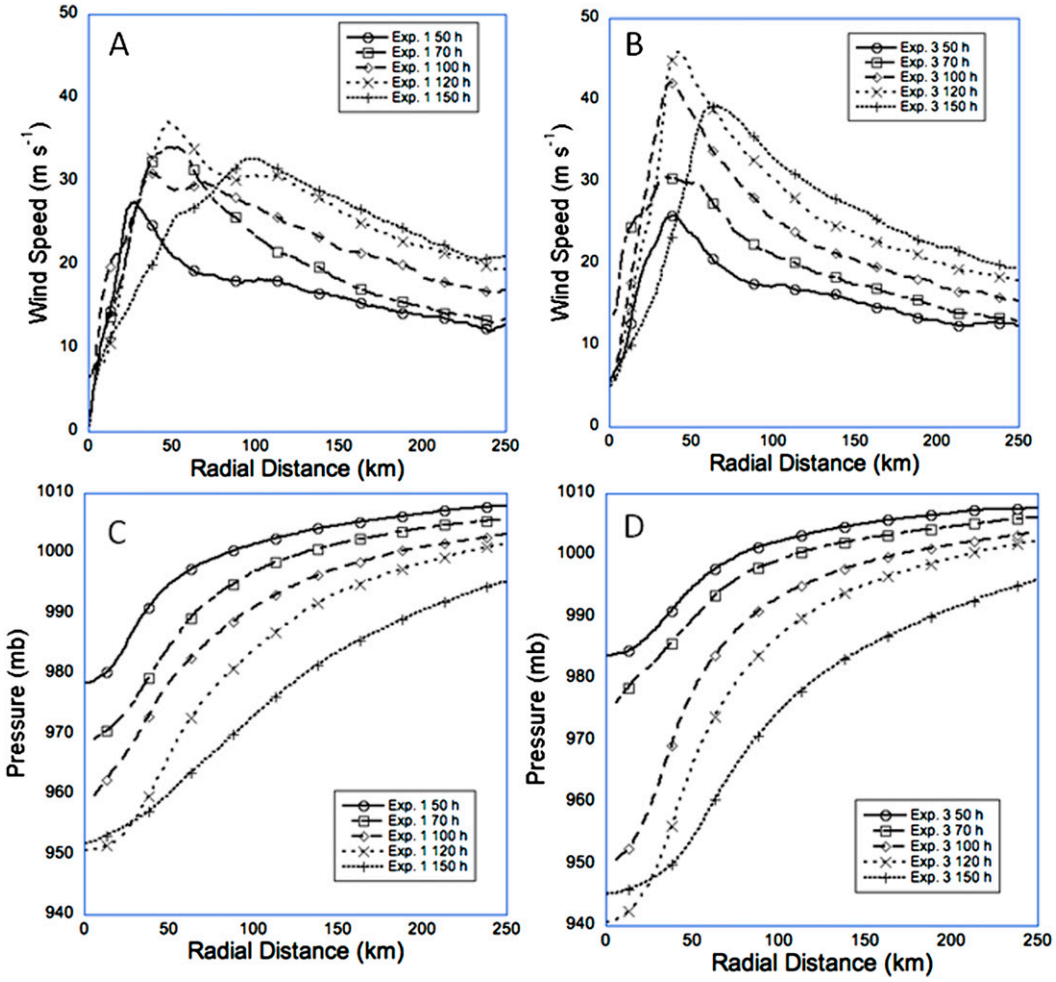

FIG. 11. (top) Radially averaged wind speed ($m\,s^{-1}$) vs radial distance for (a) Exp. 1 and (b) Exp. 3. (bottom) Radially averaged sea level pressure (mb) vs radial distance for (c) Exp. 1 and (d) Exp. 3. Experimental results are shown for hourly simulation times of 50, 70, 100, 120, and 150 h.

spacing). These times are 120 and 130 h into the simulations. The maps are plotted near the time of lowest pressure, at the height of the cirrus shield (~11 km). At the earlier time, the structure of the cloud shield in each experiment was similar to those in the other and to the observed cloud field. The circulations are relatively compact, and clouds are seen to spiral tightly around the storm center in the observations and model simulations. Yet, 12 h later, the circulation (as indicated by the color composite image) has changed dramatically. Instead of being a spiraling mass of clouds, the storm has developed two separate cloud areas: one encircling the eastern and northern quadrants around the center and one to its north. The structure and time evolution of the cirrus shield in the Exp. 1_3 km experiment shows a much better spatial agreement with the observations than the Exp. 3_3 km simulation, which mainly shows ice and aggregates encircling the simulated tropical storm center. Note that the maximum in the cloud ice content at the northern section of the hurricane is caused by aerosols that penetrated to the TC inner zone largely from the northern TC sector (not shown).

Figure 13 shows azimuthally averaged snow and graupel masses from Exp. 1_3 km and Exp. 3_3 km (with 3-km grid spacing), as well as from an experiment with uniformly continental aerosols. The snow amounts in Exp. 3_3 km (Fig. 13a) were higher than in the other experiments. Moreover, the graupel (Fig. 13b) in Exp. 3_3 km is clearly located relatively close to the TC center. The experiment with continental aerosols has less snow than Exp. 3_3 km but much more graupel than the other experiments (near the TC center), and the minimum graupel contour extends farther away from the TC center than in Exp. 3_3 km. The increase in the graupel and the decrease in the snow mass content

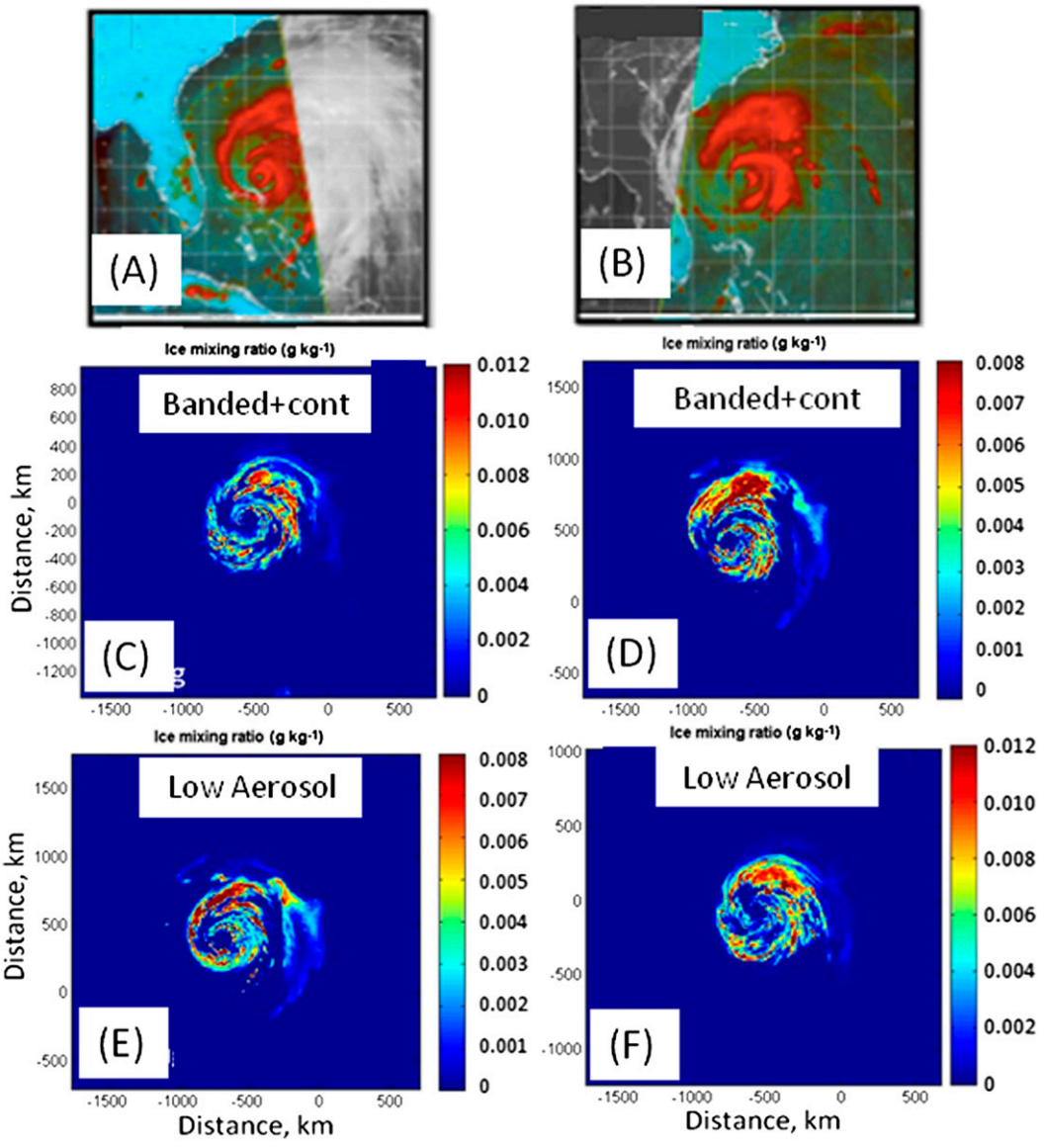

FIG. 12. (top) SSM/IS 91-GHz color composite images at (a) 2336 UTC 25 Aug and (b) 1040 UTC 26 Aug 2011. The fields of ice crystal and aggregates contents (g kg^{-1}) in the cirrus shield in a simulation with (c),(d) banded and continental vs (e),(f) uniform (low concentration) aerosols at similar times.

indicate the formation of more ''continental'' clouds characterized by the existence of more cloud water content at higher levels and more efficient conversion of snow to graupel by riming. Exp. 1_3 km had more graupel (Fig. 13c) and less snow than the experiment with maritime aerosols near the storm center because of a higher CCN concentration than in Exp. 3_3 km. Moreover, the contouring and shading in Fig. 13 shows that Exp. 1_3 km has the least compact storm circulation among the three experiments. This is the result of the effects of continental aerosols at the TC periphery, as discussed above. Thus, the effect of continental aerosols on the intensity and structure of the TC is seen in all microphysical fields.

b. Sensitivity to grid spacing

Continuous increases in computer power allow for the utilization of smaller grid spacing in cloud-resolving models. It is of interest to understand how improvements in the model resolution may affect the intensity of simulated TCs. Simulations with 3-km (or 4-km) grid spacing are often referred to as ''convection allowing'' (Clark et al. 2010). A grid spacing of 3 km is small enough to explicitly resolve convective cloud clusters

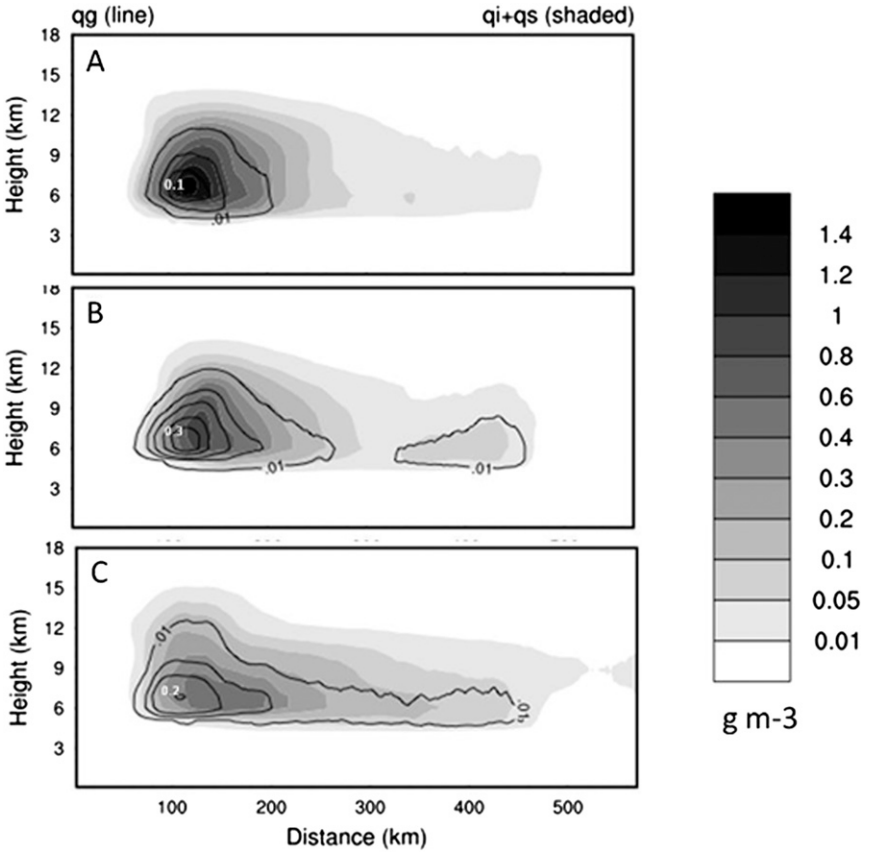

FIG. 13. Radial and 10-h time averages (g m^{-3}) between 130 and 140 h of forecast snow (shaded) and graupel (contoured) masses for initially uniform (a) low- and (b) high-concentration aerosols. (c) The results for the simulation with initially banded aerosols.

but not convective clouds. Even increasing the grid spacing to 2 km does not necessarily improve forecasts of convective systems over the United States (Schwartz et al. 2009). Schwartz et al. (2009, p. 3351) write that ''although the 2-km forecasts produced more detailed structures on the smallest resolvable scales, the patterns of convective initiation, evolution, and organization were remarkably similar to the 4-km output.'' However, Roberts and Leans (2008) note that the 4-km model representation suffers from large convective cells and delayed initiation because the grid length is too long to correctly reproduce the convection explicitly. They found that forecasts using 1-km grid spacing had better accuracy for lower threshold rainfall amounts; yet, they did not obtain better forecasts for large threshold values. In contrast, Schwartz (2014) found that their 1-km forecasts produced precipitation structures similar to those observed during their simulations of the September 2013 record-breaking rainfall over the Colorado Front Range. Hence, prior modeling results support the possibility that 1-km forecasts can more faithfully reproduce precipitation structures than their 3- or 4-km convection-allowing counterparts.

Figure 14 shows results from Exp. 1 and Exp. 2, as well as the same experiments but with 3-km grid spacing. The results indicate that simulations with 3-km resolution led to a substantially weaker storm. Maximum wind speed in Exp. 2_3 km was about 15 kt lower than in Exp. 2, while it was about 5 kt lower in Exp. 1_3 km than in Exp. 1. Both Exp. 1_3 km and Exp. 2_3 km produce their maximum wind speed about 145 h into their respective simulations. This is about 60 h later than observed. There was, however, a 20-h lag between the occurrences of the wind maximum in Exp. 1_3 km and the minimum pressure. Hence, using ocean coupling with banded aerosols with 3-km grid spacing does partially reproduce the time lag between the maximum wind and minimum pressure, but the use of the coarser grid spacings leads to large errors in the timing of both.

The plausible increase in the intensity of the TC with a decrease in grid spacing from 3 to 1 km can be derived from an analysis of microphysical fields indicating

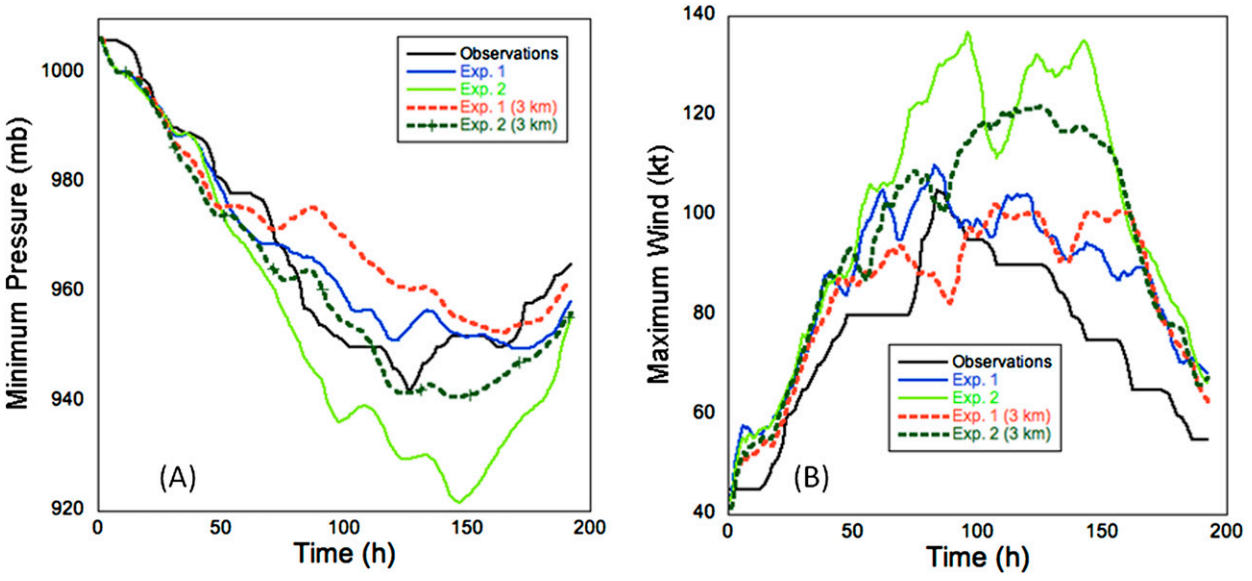

FIG. 14. As in Fig. 7, but for Exp. 1 and Exp. 2 and for Exp. 1_3 km and Exp. 2_3 km with 3-km grid spacing: (a) minimum pressure and (b) wind.

differences in the rates of latent heat release. In this sense, cloud mixing ratios [cloud water content (CWC)] is the most representative field, since the mass of cloud droplets is closely related to the process of droplet growth by condensation. Figure 15 shows vertical north–south cross sections through the TC center in the fields of CWC from Exp. 1 and Exp. 1_3 km at 0500 UTC 25 August. In both, one can see strong updrafts forming the eyewall with supercooled water that remains in clouds up to the level of homogeneous freezing (about −39°C). There is also a well-known increase in the eyewall radius with an increase in height. The simulation with 1-km grid spacing produced CWC values 50%–100% higher than those in Exp. 1_3 km. There was also an additional activated band in Exp. 1 on the northern side of the tropical storm caused by an increased concentration of aerosols in the northern TC sector during this time that was not activated in the simulation with 3-km grid spacing.

The increase in the CWC in Exp. 1 (1-km resolution), as compared to Exp. 1_3 km, was closely related to the values of vertical velocity. Because of arguments of flow

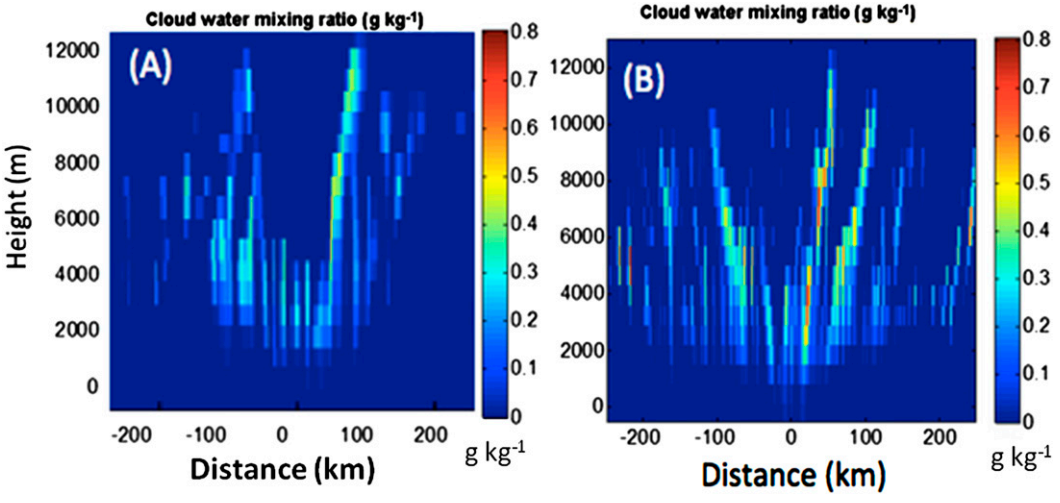

FIG. 15. Vertical north–south cross sections through the TC center of cloud mixing ratio values (g kg^{-1}) from simulations (a) Exp. 1_3 km with 3-km and (b) Exp. 1 with 1-km grid spacing with initially high concentrations of aerosol-penetrated eyewall. The southern (northern) direction is indicated by negative (positive) distances.

continuity, the vertical velocity at 1-km resolution was higher by a factor of about 1.5 than in the case of 3-km grid spacing. Higher vertical velocity leads to higher supersaturation, higher droplet concentration, and faster growth of CWC. As was shown by an analysis of heat and moisture budgets (Khain 2009), higher values of CWC indicate a higher latent heat release and higher buoyancy, which, in turn, increases vertical velocity. Thus, the increase in the grid resolution allowing for better-resolved deep convective clouds led to a more intense TC than in cases with cruder resolution. Consequently, the physics of TC intensification with a decrease in grid spacing is clear.

4. Summary and conclusions

In this study, Hurricane Irene was simulated using WRF with SBM with (mostly) 1-km spacing. One of the most intriguing features of Hurricane Irene was the 40-h time delay of minimum pressure with respect to the time of reaching maximum wind speed. During these 40 h, the decrease in maximum wind speed was accompanied by TC deepening. Such a shift indicates substantial structural changes (an increase in TC size), during which a decrease in central pressure was accompanied by a decrease in the radial pressure gradient.

To understand the reason for such a delay, the effects of two factors were tested: TC–ocean coupling and aerosol spatial distribution (including effects of continental aerosols) and grid spacing. This aspect of the storm's evolution was not simulated without taking into account the spatial distribution of aerosols, ocean feedbacks, and simulation of cloud-scale processes on a grid with 1-km grid spacing. It was found that the 40-h time delay of minimum pressure with respect to the time of reaching maximum of wind speed was related to an aerosol-induced formation of the secondary eyewall at a larger distance from the TC center and a dissipation of the old eyewall. Such fine reconstruction of the inner-core TC structure requires high grid resolution and accurate representation of cloud microphysical processes, especially aerosol-induced convection invigoration.

It was shown that in the simulation that included the effects of Sahara dust and continental aerosols (with ocean coupling), both the TC structure (cirrus shield, structure, and rainbands) and intensity were more similar to observations than a simulation with uniform spatial aerosol distributions. The microphysical structure (hydrometeor mass and concentrations) and the area and location of the cirrus shield were all largely determined by aerosols activated into CCN.

An analysis of the simulation during the period of time shift between the maximum wind and the minimum pressure in TC Irene showed that aerosols that penetrated the TC inner region (during the period when a TC crossed the dust band) invigorated convection and intensified it. However, aerosols also intensified convection at the outer periphery of the eyewall and rainbands in the vicinity of the eyewall. This, in turn, led to an increase in the radius of the eyewall and to an increase in the TC size. Continuous penetration of aerosols to the TC periphery from the continental United States led to a further intensification of convection at the TC periphery as well as to a further increase in TC size and further relative weakening. Our results showed that the intensification of the secondary eyewall and formation and intensification of rainbands at the TC periphery was the main factor in the time shift between maximum wind and minimum surface pressure, as long as there was ocean coupling. The weakening effect of high concentration (mainly land-based aerosols) dominated at the mature and decaying stages, resulting in an increase in the minimum pressure by 10–15 mb and to a decrease in the maximum wind by 15–25 kt in the mature hurricane compared to the simulation with uniform aerosols. The differences in the maximum wind speed were about two-thirds of those caused by not including TC–ocean coupling (with the same initial banded aerosols and aerosols over land). Moreover, the results highlight the importance of knowing aerosol concentration, not only near land but also over the open ocean, for the correct prediction of TC evolution.

It was also found that an increase in the grid resolution from 3 to 1 km led to an intensification of simulated TC. These conclusions accord with those reported by Gopalakrishnan et al. (2011, 2012). This intensification can be attributed to a better approximation of convective processes, which led to an increase in the vertical velocity in simulated clouds and a corresponding simulated increase in the latent heat release. Without ocean mixing, the simulated storms at 1 km were found to have maximum wind and minimum pressure higher and lower than observed, respectively. It is interesting that aerosol impacts on the time lag between maximum wind and minimum pressure manifested themselves so strongly when there was TC–ocean coupling. Yet we noted that the double maximum in the maximum wind–minimum pressure curve (Fig. 8) from Exp. 2 may indicate transient effects of aerosols on the storm development. Note that effects of the TC–ocean coupling tend to weaken the TC and to increase its size. This is because convection tends to develop over zones with high sea surface temperatures at higher distances from the TC center. The aerosol-induced intensification of convection at the TC periphery also leads to a TC weakening and an increase in the TC size. So it was necessary to use a

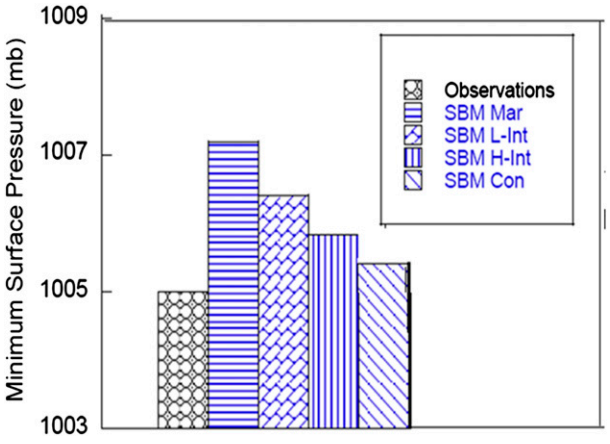

FIG. 16. Histogram of the minimum surface pressure in TD Debbie (2006) simulated at low (SBM-MAR) and high (SBM-CON) CCN concentrations, as well as two intermediate concentrations: L-Int and H-Int.

high-resolution SBM model that is sensitive to aerosols and to take into account the TC–ocean coupling and effects of continental aerosols to reproduce the 40-h time delay of minimum pressure with respect to the time of reaching maximum wind speed.

Note that the results of Herbener et al. (2014), who showed the intensification of an idealized developing hurricane when aerosols penetrated its inner core, are consistent with our results. The process of aerosol-induced intensification should be especially pronounced in the case of tropical depressions (TD), when significant aerosol concentrations may occur in the TD core. As an example, Fig. 16 shows a histogram of the minimum pressure in TD Debbie at 1800 UTC 22 August 2006, 3 days after the initial forecast time, from supplemental simulations using the same model WRF-SBM. Simulations were performed at low [SBM with maritime aerosols (SBM-MAR)], high [SBM with continental aerosols (SBM-CON)], and two intermediate CCN concentrations: low intermediate (L-Int) and high intermediate (H-Int). An increase in the aerosol concentration in the area of the TD location accelerated the TD development and brought the TD-simulated minimum pressure more in line with the observed one. These results are consistent with those of Jiang (2012), who demonstrated a high correlation between the intensity of convection in the inner core of a TC and its intensification.

The potentially important effect of sea spray produced in the TC inner core on TC microphysics and intensity was not taken into account in these simulation experiments. As was shown by Shpund et al. (2011, 2012, 2014), large eddies in the boundary layer are able to raise sea-spray drops with diameters as large as several hundred microns to altitudes of a few hundred meters. These sea-spray drops, which are the size of raindrops, may ascend in deep convective clouds, thus accelerating the process of collisions. The presence of small aerosols (from sea spray or background aerosols) can lead to a synergetic effect, leading to intense in-cloud nucleation, intensification of lightning, and other consequences (Khain et al. 2012). We plan to investigate the effects of sea spray on tropical storms in future studies.

Acknowledgments. This research was supported by the U.S. Department of Energy's Atmospheric Science Program, Atmospheric System Research, and the Office of Science, Office of Biological and Environmental Research program under Grants DE-SC0006788 and DE-SC0008811, as well as by the Binational United States–Israel Science Foundation (Grant 2010446). We acknowledge the Department of Energy for granting us access to their supercomputing cluster. We would also like to thank NOAA's ESRL for providing computing for preliminary simulations studies and the NCDC for providing us with GFS reanalysis data.

REFERENCES

Avila, L. A., and J. Cangialosi, 2011: Hurricane Irene. National Hurricane Center Tropical Cyclone Rep. AL092011, 45 pp. [Available online at http://www.nhc.noaa.gov/data/tcr/AL092011_Irene.pdf.]

Bender, M. A., and I. Ginis, 2000: Real-case simulations of hurricane–ocean interaction using a high-resolution coupled model: Effects on hurricane intensity. *Mon. Wea. Rev.*, **128**, 917–946, doi:10.1175/1520-0493(2000)128<0917:RCSOHO>2.0.CO;2.

——, ——, and Y. Kurihara, 1993: Numerical simulations of hurricane–ocean interaction with a high-resolution coupled model. *J. Geophys. Res.*, **98**, 23 245–23 263, doi:10.1029/93JD02370.

Bigg, E. K., 1953: The formation of atmospheric ice crystals by the freezing of droplets. *Quart. J. Roy. Meteor. Soc.*, **79**, 510–519, doi:10.1002/qj.49707934207.

Chen, H., D.-L. Zhang, J. Carton, and R. Atlas, 2011: On the rapid intensification of Hurricane Wilma (2005). Part I: Model prediction and structural changes. *Wea. Forecasting*, **26**, 885–901, doi:10.1175/WAF-D-11-00001.1.

Clark, A. J., W. A. Gallus Jr., and M. L. Weisman, 2010: Neighborhood-based verification of precipitation forecasts from convection-allowing NCAR WRF Model simulations and the operational NAM. *Wea. Forecasting*, **25**, 1495–1509, doi:10.1175/2010WAF2222404.1.

Cotton, W. R., H. Zhang, G. M. McFarquhar, and S. M. Saleeby, 2007: Should we consider polluting hurricanes to reduce their intensity? *J. Wea. Modif.*, **39**, 70–73.

——, G. M. Krall, and G. G. Carrió, 2012: Potential indirect effects of aerosol on tropical cyclone intensity: Convective fluxes and cold-pool activity. *Trop. Cyclone Res. Rev.*, **1**, 293–306, doi:10.6057/2012TCRR03.05.

Davis, C., and Coauthors, 2008: Prediction of landfalling hurricanes with the Advanced Hurricane WRF Model. *Mon. Wea. Rev.*, **136**, 1990–2005, doi:10.1175/2007MWR2085.1.

Fierro, A. O., R. F. Rogers, F. D. Marks, and D. S. Nolan, 2009: The impact of horizontal grid spacing on the microphysical and kinematic structures of strong tropical cyclones simulated with the WRF-ARW Model. *Mon. Wea. Rev.*, **137**, 3717–3743, doi:10.1175/2009MWR2946.1.

Gopalakrishnan, S. G., F. Marks, X. Zhang, J.-W. Bao, K.-S. Yeh, and R. Atlas, 2011: The experimental HWRF system: A study on the influence of horizontal resolution on the structure and intensity changes in tropical cyclones using an idealized framework. *Mon. Wea. Rev.*, **139**, 1762–1784, doi:10.1175/2010MWR3535.1.

——, S. Goldenberg, T. Quirino, X. Zhang, F. Marks, K.-S. Yeh, R. Atlas, and V. Tallapragada, 2012: Toward improving high-resolution numerical hurricane forecasting: Influence of model horizontal grid resolution, initialization, and physics. *Wea. Forecasting*, **27**, 647–666, doi:10.1175/WAF-D-11-00055.1.

Hazra, A., P. Mukhopadhyay, S. Taraphdar, J.-P. Chen, and W. R. Cotton, 2013: Impact of aerosols on Tropical cyclones: An investigation using convection-permitting model simulation. *J. Geophys. Res. Atmos.*, **118**, 7157–7168, doi:10.1002/jgrd.50546.

Herbener, S. R., S. C. Van den Heever, G. G. Carrió, S. M. Saleeby, and W. R. Cotton, 2014: Aerosol indirect effects on idealized tropical cyclone dynamics. *J. Atmos. Sci.*, **71**, 2040–2055, doi:10.1175/JAS-D-13-0202.1.

Jenkins, G. S., and A. Pratt, 2008: Saharan dust, lightning and tropical cyclones in the eastern tropical Atlantic during NAMMA-06. *Geophys. Res. Lett.*, **35**, L12804, doi:10.1029/2008GL033979.

——, A. S. Pratt, and A. Heymsfield, 2008: Possible linkages between Saharan dust and tropical cyclone rain band invigoration in the eastern Atlantic during NAMMA-06. *Geophys. Res. Lett.*, **35**, L08815, doi:10.1029/2008GL034072.

Jiang, H., 2012: The relationship between tropical cyclone intensity change and the strength of inner-core convection. *Mon. Wea. Rev.*, **140**, 1164–1176, doi:10.1175/MWR-D-11-00134.1.

Khain, A. P., 1984: *Mathematical Modeling of Tropical Cyclones.* Gidrometeoizdat, 247 pp.

——, 2009: Notes on state-of-the-art investigations of aerosol effects on precipitation: A critical review. *Environ. Res. Lett.*, **4**, 015004, doi:10.1088/1748-9326/4/1/015004.

——, and G. G. Sutyrin, 1983: *Tropical Cyclones and Their Interaction with the Ocean.* Gidrometeoizdat, 241 pp.

——, and B. Lynn, 2011: Simulation of tropical cyclones using a mesoscale model with spectral bin microphysics. *Recent Hurricane Research—Climate, Dynamics, and Societal Impacts*, A. R. Lupo, Ed., Intech, 197–227, doi:10.5772/15907.

——, M. Ovtchinnikov, M. Pinsky, A. Pokrovsky, and H. Krugliak, 2000: Notes on the state-of-the-art numerical modeling of cloud microphysics. *Atmos. Res.*, **55**, 159–224, doi:10.1016/S0169-8095(00)00064-8.

——, M. B. Pinsky, M. Shapiro, and A. Pokrovsky, 2001: Collision rate of small graupel and water drops. *J. Atmos. Sci.,* **58**, 2571–2595, doi:10.1175/1520-0469(2001)058<2571:CROSGA>2.0.CO;2.

——, A. Pokrovsky, M. Pinsky, A. Seifert, and V. Phillips, 2004: Effects of atmospheric aerosols on deep convective clouds as seen from simulations using a spectral microphysics mixed-phase cumulus cloud model. Part I: Model description. *J. Atmos. Sci.*, **61**, 2963–2982, doi:10.1175/JAS-3350.1.

——, D. Rosenfeld, and A. Pokrovsky, 2005: Aerosol impact on the dynamics and microphysics of convective clouds. *Quart. J. Roy. Meteor. Soc.*, **131**, 2639–2663, doi:10.1256/qj.04.62.

——, N. BenMoshe, and A. Pokrovsky, 2008a: Factors determining the impact of aerosols on surface precipitation from clouds: An attempt at classification. *J. Atmos. Sci.*, **65**, 1721–1748, doi:10.1175/2007JAS2515.1.

——, N. Cohen, B. Lynn, and A. Pokrovsky, 2008b: Possible aerosol effects on lightning activity and structure of hurricanes. *J. Atmos. Sci.*, **65**, 3652–3667, doi:10.1175/2008JAS2678.1.

——, B. Lynn, and J. Dudhia, 2010: Aerosol effects on intensity of landfalling hurricanes as seen from simulations with the WRF Model with spectral bin microphysics. *J. Atmos. Sci.*, **67**, 365–384, doi:10.1175/2009JAS3210.1.

——, V. Phillips, N. Benmoshe, and A. Pokrovsky, 2012: The role of small soluble aerosols in the microphysics of deep maritime clouds. *J. Atmos. Sci.*, **69**, 2787–2807, doi:10.1175/2011JAS3649.1.

Ma, Z., J. Fei, L. Liu, X. Huang, and X. Cheng, 2013: Effects of the cold core eddy on tropical cyclone intensity and structure under idealized air–sea interaction conditions. *Mon. Wea. Rev.*, **141**, 1285–1303, doi:10.1175/MWR-D-12-00123.1.

Meyers, M. P., P. J. DeMott, and W. R. Cotton, 1992: New primary ice-nucleation parameterizations in an explicit cloud model. *J. Appl. Meteor.*, **31**, 708–721, doi:10.1175/1520-0450(1992)031<0708:NPINPI>2.0.CO;2.

Nakanishi, M., 2000: Large-eddy simulation of radiation fog. *Bound.-Layer Meteor.*, **94**, 461–493, doi:10.1023/A:1002490423389.

——, and H. Niino, 2009: Development of an improved turbulence closure model for the atmospheric boundary layer. *J. Meteor. Soc. Japan*, **87**, 895–912, doi:10.2151/jmsj.87.895.

Pinsky, M., A. P. Khain, and M. Shapiro, 2001: Collision efficiency of drops in a wide range of Reynolds numbers: Effects of pressure on spectrum evolution. *J. Atmos. Sci.*, **58**, 742–764, doi:10.1175/1520-0469(2001)058<0742:CEODIA>2.0.CO;2.

Pollard, R. T., P. B. Rhines, and R. O. R. Y. Thompson, 1972: The deepening of the wind-mixed layer. *Geophys. Fluid Dyn.*, **4**, 381–404, doi:10.1080/03091927208236105.

Roberts, N. M., and H. W. Lean, 2008: Scale-selective verification of rainfall accumulations from high-resolution forecasts of convective events. *Mon. Wea. Rev.*, **136**, 78–97, doi:10.1175/2007MWR2123.1.

Rosenfeld, D., U. Lohmann, G. B. Raga, C. D. O'Dowd, M. Kulmala, S. Fuzzi, A. Reissell, and M. O. Andreae, 2008: Flood or drought: How do aerosols affect precipitation? *Science*, **321**, 1309–1313, doi:10.1126/science.1160606.

——, W. L. Woodley, A. Khain, W. R. Cotton, G. Carrió, I. Ginis, and J. H. Golden, 2012: Aerosol effects on microstructure and intensity of tropical cyclones. *Bull. Amer. Meteor. Soc.*, **93**, 987–1001, doi:10.1175/BAMS-D-11-00147.1.

Schwartz, C. S., 2014: Reproducing the September 2013 record-breaking rainfall over the Colorado front range with high-resolution WRF forecasts. *Wea. Forecasting*, **29**, 393–402, doi:10.1175/WAF-D-13-00136.1.

——, and Coauthors, 2009: Next-day convection-allowing WRF Model guidance: A second look at 2-km versus 4-km grid spacing. *Mon. Wea. Rev.*, **137**, 3351–3372, doi:10.1175/2009MWR2924.1.

Shpund, J., M. Pinsky, and A. Khain, 2011: Microphysical structure of the marine boundary layer under strong wind and spray formation as seen from simulations using a 2D

explicit microphysical model. Part I: The impact of large eddies. *J. Atmos. Sci.*, **68**, 2366–2384, doi:10.1175/2011JAS3652.1.

——, J. A. Zhang, M. Pinsky, and A. Khain, 2012: Microphysical structure of the marine boundary layer under strong wind and spray formation as seen from simulations using a 2D explicit microphysical model. Part II: The role of sea spray. *J. Atmos. Sci.*, **69**, 3501–3514, doi:10.1175/JAS-D-11-0281.1.

——, ——, ——, and ——, 2014: Microphysical structure of the marine boundary layer under strong wind and spray formation as seen from a 2D explicit microphysical model. Part III: Parameterization of height-dependent droplet size distribution. *J. Atmos. Sci.*, **71**, 1914–1934, doi:10.1175/JAS-D-12-0201.1.

Skamarock, W. C., and J. B. Klemp, 2008: A time-split nonhydrostatic atmospheric model for weather research and forecasting applications. *J. Comput. Phys.*, **227**, 3465–3485, doi:10.1016/j.jcp.2007.01.037.

Tao, W.-K., J.-P. Chen, Z. Li, C. Wang, and C. Zhang, 2012: Impact of aerosols on convective clouds and precipitation. *Rev. Geophys.*, **50**, RG2001, doi:10.1029/2011RG000369.

Telegraph, 2011: 'Dangerous' Hurricane Irene becomes 'big threat' to US as evacuations begin. *Telegraph*, 25 August. [Available online at http://www.telegraph.co.uk/news/worldnews/northamerica/usa/8721766/Dangerous-Hurricane-Irene-becomes-big-threat-to-US-as-evacuations-begin.html.]

Vali, G., 1994: Freezing rate due to heterogeneous nucleation. *J. Atmos. Sci.*, **51**, 1843–1856, doi:10.1175/1520-0469(1994)051<1843:FRDTHN>2.0.CO;2.

Wang, Y., 2009: How do outer spiral rainbands affect tropical cyclone structure and intensity? *J. Atmos. Sci.*, **66**, 1250–1273, doi:10.1175/2008JAS2737.1.

Zhang, H., G. M. McFarquhar, W. R. Cotton, and Y. Deng, 2009: Direct and indirect impacts of Saharan dust acting as cloud condensation nuclei on tropical cyclone eyewall development. *Geophys. Res. Lett.*, **36**, L06802, doi:10.1029/2009GL037276.

Zhou, X., and B. Wang, 2011: Mechanism of concentric eyewall replacement cycles and associated intensity change. *J. Atmos. Sci.*, **68**, 972–988, doi:10.1175/2011JAS3575.1.

——, ——, X. Ge, and T. Li, 2011: Impact of secondary eyewall heating on tropical cyclone intensity change. *J. Atmos. Sci.*, **68**, 450–456, doi:10.1175/2010JAS3624.1.